

## Hydrothermal Growth of Mesoporous SBA-15 Silica in the Presence of PVP-Stabilized Pt Nanoparticles: Synthesis, Characterization, and Catalytic Properties

Hyunjoon Song,<sup>†</sup> Robert M. Rioux, James D. Hoefelmeyer,<sup>‡</sup> Russell Komor, Krisztian Niesz, Michael Grass, Peidong Yang,<sup>\*</sup> and Gabor A. Somorjai<sup>\*</sup>

Contribution from the Department of Chemistry, University of California, Berkeley, and Lawrence Berkeley National Laboratory, Materials and Chemical Sciences Divisions, Berkeley, California 94720

Received October 29, 2005; E-mail: p\_yang@berkeley.edu; somorjai@berkeley.edu.

**Abstract:** A novel high surface area heterogeneous catalyst based on solution phase colloidal nanoparticle chemistry has been developed. Monodisperse platinum nanoparticles of 1.7–7.1 nm have been synthesized by alcohol reduction methods and incorporated into mesoporous SBA-15 silica during hydrothermal synthesis. Characterization of the Pt/SBA-15 catalysts suggests that Pt particles are located within the surfactant micelles during silica formation leading to their dispersion throughout the silica structure. After removal of the templating polymer from the nanoparticle surface, Pt particle sizes were determined from monolayer gas adsorption measurements. Infrared studies of CO adsorption revealed that CO exclusively adsorbs to atop sites and red-shifts as the particle size decreases suggesting surface roughness increases with decreasing particle size. Ethylene hydrogenation rates were invariant with particle size and consistent with a clean Pt surface. Ethane hydrogenolysis displayed significant structure sensitivity over the size range of 1–7 nm, while the apparent activation energy increased linearly up to a Pt particle size of ~4 nm and then remained constant. The observed rate dependence with particle size is attributed to a higher reactivity of coordinatively unsaturated surface atoms in small particles compared to low-index surface atoms prevalent in large particles. The most reactive of these unsaturated surface atoms are responsible for ethane decomposition to surface carbon. The ability to design catalytic structures with tunable properties by rational synthetic methods is a major advance in the field of catalyst synthesis and for the development of accurate structure–function relationships in heterogeneous reaction kinetics.

### 1. Introduction

One of the goals of modern catalysis research is to design catalysts capable of near 100% selectivity for the desired product without sacrificing activity and energy consumption.<sup>1,2</sup> The role of each component in these catalysts,<sup>3</sup> i.e., metal particles,<sup>4</sup> oxide supports,<sup>5</sup> and their interface<sup>6</sup> must be understood, requiring not only catalyst synthesis but characterization and performance in designated catalytic reactions (reactivity studies). To this end, there is a drive toward developing new strategies to synthesize catalysts whose catalytic performance can be predicted in a defined and rational manner. Parameters to control in transition metal heterogeneous catalysts include particle composition, size, and shape; support composition and pore size distribution; and the organizational structure of the porous network. This

multidimensional problem is complex; thus, the synthetic control and design of catalysts is a serious technological challenge.<sup>7–9</sup> A logical approach to the problem is to isolate one of the parameters and learn how to control it in a systematic way and then test its effect on catalytic performance.

Several methods have been developed thus far to afford the effective immobilization of metal particles on high surface area support materials.<sup>10,11</sup> The most prominent methods are incipient wetness and ion exchange, in which the porous oxide support is impregnated with metal precursors (simple salts) in solution phase, followed by thermal treatment and/or reduction with H<sub>2</sub> to form metal nanoparticles.<sup>6,12,13</sup> The process can be further refined by postsynthesis modification of the support surface functionalization which directs the interaction of precursor with

<sup>†</sup> Current address: Department of Chemistry and School of Molecular Science (BK21), Korea Advanced Institute of Science and Technology, Daejeon, 305-701, Korea.

<sup>‡</sup> Current address: Department of Chemistry, University of South Dakota, Vermillion, SD 57069.

(1) Somorjai, G. A.; Borodko, Y. G. *Catal. Lett.* **2001**, *76*, 1.

(2) Bell, A. T. *Science* **2003**, *299*, 1688.

(3) Grunes, J.; Zhu, J.; Somorjai, G. A. *Chem. Commun.* **2003**, *18*, 2257.

(4) Boudart, M. J. *Mol. Catal.* **1985**, *30*, 27.

(5) Rolison, D. R. *Science* **2003**, *299*, 1698.

(6) Hayek, K.; Kramer, R.; Paál, Z. *Appl. Catal., A* **1997**, *162*, 1.

(7) Kung, H. H.; Kung, M. C. *Appl. Catal., A* **2003**, *246*, 193.

(8) Kung, H. H.; Kung, M. C. *Top. Catal.* **2005**, *34*, 77.

(9) Schlögl, R.; Hamid, S. B. A. *Angew. Chem., Int. Ed.* **2004**, *43*, 1628.

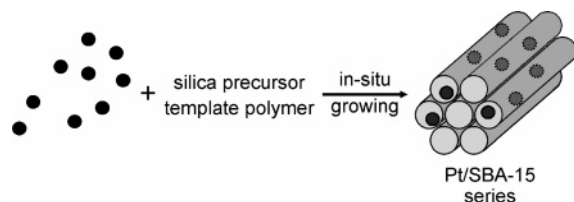
(10) Ertl, G.; Knözinger, H.; Weitkamp, J. *Handbook of Heterogeneous Catalysis*; Wiley/VCH: New York/Weinheim, 1997.

(11) Geus, J. W.; van Ween, J. A. R. *Catalysis: An Integrated Approach to Homogeneous, Heterogeneous and Industrial Catalysis*; Moulijn, J. A., van Leeuwen, P. W. N. M., van Santen, R. A., Eds.; Elsevier: Amsterdam, 1993; Chapter 9.

(12) Fukuoka, A.; Higashimoto, N.; Sakamoto, Y.; Inagaki, S.; Fukushima, Y.; Ichikawa, M. *Top. Catal.* **2002**, *18*, 73.

(13) Yang, C.-M.; Liu, P.-H.; Chiu, C.-Y.; Chao, K.-J. *Chem. Mater.* **2003**, *15*, 275.

**Scheme 1.** Schematic of Nanoparticle Encapsulation (NE) Method for Catalyst Synthesis



the surface.<sup>14</sup> Due to its simplicity and crude effectiveness, this method is successful for the large scale production of catalysts; however, metal nanoparticles generated on the support typically lack uniformity in size and shape.

The discovery of M41S-type ordered mesoporous materials opened a new class of periodic porous solids.<sup>15</sup> Mesoporous silica structures have been regarded as ideal supports for heterogeneous catalysts due to their high surface area, tunable pore size, and alignment. In particular, the SBA-15 framework synthesized by Zhao et al.<sup>16</sup> has a highly ordered hexagonal mesostructure with parallel channels and adjustable pore size in the range of 5–30 nm.<sup>17</sup> This size regime is relevant to catalysis, since the catalytically active components are metal particles in the 1–10 nm size range. SBA-15 is well suited as a structure that can contain individual metal particles within its mesopores, and the pores are wide enough to permit facile diffusion of reactants and products.

With the use of the periodic SBA-15 structure, a general approach for the design of high surface area catalysts is demonstrated. Departing from traditional catalyst preparation methods, well-defined Pt nanocrystals have been synthesized in the presence of surface-templating agents by a solution-based technique. The size and shape of the nanoparticles are uniform and tunable in the range of 1.7–8 nm. We have recently reported particle incorporation in SBA-15 by sonication, denoted CI, for capillary inclusion.<sup>18</sup> The Pt particles were well-dispersed within the entire silica framework, and the resulting Pt/SBA-15 catalysts demonstrated reasonable reactivity during ethylene hydrogenation and ethane hydrogenolysis. A large fraction of the active Pt nanoparticles are potentially located on the SBA-15 outer surface as well as inside the channels, and the maximum Pt particle size incorporated in the mesopores is restricted by the channel diameter of SBA-15 (~9 nm). An alternative approach is the encapsulation of nanoparticles during in situ growth of SBA-15 (Scheme 1), denoted NE (nanoparticle encapsulation). Polymers are effective mediators for organizing nanoparticles into higher order composite structures.<sup>19</sup> Somorjai and co-workers recently demonstrated the growth of SBA-15 on the surface of Pt cubes.<sup>20,21</sup> Hexagonal silica structures were formed by adding Pluronic P123 (triblock copolymer poly-

(ethylene oxide)–poly(propylene oxide)–poly(ethylene oxide), EO<sub>20</sub>PO<sub>70</sub>EO<sub>20</sub>) and tetraethoxysilane (TEOS) to the Pt hydrosol in acidic condition. The final Pt/SBA-15 composite, however, exhibited no catalytic activity.

The extremely low pH required for synthesis of SBA-15 disrupts the Pt colloid; however, the use of a pH neutral template would allow incorporation of the Pt sol. The MSU family of high surface area ordered mesoporous silica materials are synthesized at neutral pH, and utilize triblock polymers, which template SBA-15 synthesis, to obtain similar pore diameter.<sup>22</sup> Therefore, we introduce a synthetic procedure to generate hexagonal structures in neutral pH conditions in the presence of Pt nanoparticles. The resulting Pt nanocrystal/SBA-15 materials possess an ordered silica structure with improved dispersion of Pt nanoparticles in its channels. These nanocomposites exhibit comparable catalytic behavior to that of conventional catalysts after removal of the organic residues (polymer template and surface-templating agent of Pt sol) by heat treatment. Precise tuning of particle size and support structures will enable the elucidation of their contribution to the overall kinetic (activity and selectivity) behavior of a heterogeneous catalyst.

## 2. Experimental Section

**2.1. Synthesis of Pt Nanoparticles.** Dihydrogen hexachloroplatinate (H<sub>2</sub>PtCl<sub>6</sub>·6H<sub>2</sub>O, 99.9%, metals basis) was purchased from Alfa Aesar. Poly(vinylpyrrolidone) (PVP, *M<sub>w</sub>* = 29 000 and 55 000) was obtained from Sigma-Aldrich. Methanol, ethanol, and ethylene glycol were of analytical grade and used without further purification.

Pt particles were synthesized according to literature methods.<sup>18,23,24</sup> Briefly, 1.7 nm Pt particles were made by adding NaOH solution (12.5 mL, 0.5 M) in ethylene glycol to a solution of H<sub>2</sub>PtCl<sub>6</sub>·6H<sub>2</sub>O (250 mg) in 12.5 mL of ethylene glycol. The mixture was heated at 433 K for 3 h with N<sub>2</sub> bubbling. After reaction, particles were precipitated by adding 1 mL of 2 M HCl and dispersed in ethanol containing 12.2 mg of PVP (*M<sub>w</sub>* = 29 000). The 2.9 nm Pt particles were synthesized by refluxing a mixture of PVP (26.6 mg) and H<sub>2</sub>PtCl<sub>6</sub>·6H<sub>2</sub>O (124.3 mg) in water (40 mL)/methanol (360 mL) solution for 3 h. The 3.6 nm Pt particles were formed by mixing the 2.9 nm Pt colloidal solution (100 mL) in a water/methanol (1:9) mixture with 10 mL of 6.0 mM H<sub>2</sub>PtCl<sub>6</sub>·6H<sub>2</sub>O aqueous solution and 90 mL of methanol. The mixture was refluxed for 3 h. The 7.1 nm Pt particles were synthesized by adding a total 3 mL of 0.375 M PVP (*M<sub>w</sub>* = 55 000) and 1.5 mL of 0.0625 M H<sub>2</sub>PtCl<sub>6</sub>·6H<sub>2</sub>O solutions in refluxing ethylene glycol every 30 s over 16 min. The mixture was refluxed for an additional 5 min.

All Pt colloidal solutions were purified by sequential precipitation/redispersion and eventually dispersed in an appropriate amount of deionized water necessary for a 3 × 10<sup>-3</sup> M solution based on Pt salt concentration. The particle sizes were measured by transmission electron microscopy (TEM) and X-ray diffraction (XRD). Estimated particle sizes were 1.73 ± 0.26 (1.7), 2.80 ± 0.21 (2.9), 3.39 ± 0.26 (3.6), and 7.16 ± 0.37 (7.1) nm by TEM (XRD), respectively, indicating high uniformity and monodispersity of each particle less than σ ~ 8%.<sup>18</sup>

**2.2. Synthesis of the Pt/SBA-15 Series by the Nanoparticle Encapsulation (NE) Method.** Pluronic P123 (EO<sub>20</sub>PO<sub>70</sub>EO<sub>20</sub>, BASF), tetramethyl orthosilicate (TMOS, 98%, Aldrich), and sodium fluoride (99.99%, Aldrich) were used as received. An amount of 2.5 g of Pluronic P123 was completely dissolved in 50.5 mL of deionized water. The Pt colloidal aqueous solution (27.0 mL, 3 × 10<sup>-3</sup> M) was mixed

(14) Fukuoka, A.; Araki, H.; Sakamoto, Y.; Sugimoto, N.; Tsukada, H.; Kumai, Y.; Akimoto, Y.; Ichikawa, M. *Nano Lett.* **2002**, *2*, 793.

(15) Kresge, C. T.; Leonowicz, M. E.; Roth, W. J.; Vartuli, J. C.; Beck, J. S. *Nature* **1992**, *359*, 710.

(16) Zhao, D.; Feng, J.; Huo, Q.; Melosh, N.; Fredrickson, G. H.; Chmelka, B. F.; Stucky, G. D. *Science* **1998**, *279*, 548.

(17) Zhao, D.; Huo, Q.; Feng, J.; Chmelka, B. F.; Stucky, G. D. *J. Am. Chem. Soc.* **1998**, *120*, 6024.

(18) Rioux, R. M.; Song, H.; Hoefelmeyer, J. D.; Yang, P. D.; Somorjai, G. A. *J. Phys. Chem. B* **2005**, *109*, 2192.

(19) Shenhar, R.; Norsten, T. B.; Rotello, V. M. *Adv. Mater.* **2005**, *17*, 657.

(20) Kónya, Z.; Puentes, V. F.; Kiricsi, I.; Zhu, J.; Alivisatos, A. P.; Somorjai, G. A. *Nano Lett.* **2002**, *2*, 907.

(21) Zhu, J.; Kónya, Z.; Puentes, V. F.; Kiricsi, I.; Miao, C. X.; Ager, J. W.; Alivisatos, A. P.; Somorjai, G. A. *Langmuir* **2003**, *19*, 4396.

(22) Bagshaw, S. A.; Prouzet, E.; Pinnavaia, T. J. *Science* **1995**, *269*, 1242.

(23) Wang, Y.; Ren, J.; Deng, K.; Gui, L.; Tang, Y. *Chem. Mater.* **2000**, *12*, 1622.

(24) Teranishi, T.; Hosoe, M.; Tanaka, T.; Miyake, M. *J. Phys. Chem. B* **1999**, *103*, 3818.

with the polymer solution and stirred for 1 h at 313 K. A volume of 0.375 mL of 0.5 M NaF aqueous solution was added, and 3.91 mL of TMOS was quickly added to the reaction mixture, followed by stirring for a day at 313 K. The resulting slurry was aged for an additional day at 373 K. The brown precipitates were separated by centrifugation, thoroughly washed with ethanol, and dried in an oven at 373 K. Pt(1.7 nm)/SBA-15 was calcined at 623 K for 24 h, Pt(7.1 nm)/SBA-15 was calcined at 723 K for 36 h, and other catalyst materials were calcined at 723 K for 24 h under O<sub>2</sub> flow.

A 3.2% Pt/SiO<sub>2</sub><sup>25</sup> and a 6.3% Pt/SiO<sub>2</sub> (EUROPT-1) catalyst prepared by an ion-exchange method were used as reference materials. The EUROPT-1 sample has been thoroughly characterized.<sup>26–30</sup> The Pt particle size distribution is 1–3.5 nm centered at 1.8 nm with 75% of the particles having a diameter of  $\leq 2$  nm.<sup>27</sup> Turnover frequencies of ethylene hydrogenation on the 3.2% Pt/SiO<sub>2</sub> have been previously reported;<sup>18</sup> these rates were a factor of 5 lower than those reported here. This discrepancy is attributed to errors in extrapolation from low-temperature conditions used in the previous study to room-temperature conditions. All turnover frequencies reported in this study were reproducible to  $\pm 10\%$ .

**2.3. Characterization of Pt/SBA-15 Catalysts. 2.3.1. Physical and Chemical Characterization.** TEM experiments were carried out on a Philips CM200 microscope operated at 200 kV at the National Center for Electron Microscopy at Lawrence Berkeley National Laboratory. Catalysts were sonicated in acetone for 10 s, dropped on lacey carbon film coated copper grids (Ted Pella), and dried in air. Water contact angle measurements were performed on a CAM 100 optical contact angle meter (KSY Instruments). Polymer and Pt nanoparticle solutions in ethanol were dropped on Si substrates and dried under vacuum for 8 h. The preparation of Pt Langmuir–Blodgett (LB) monolayers for contact angle measurements has been described elsewhere.<sup>31</sup>

XRD patterns were measured on a Bruker D8 GADDS diffractometer using Co K $\alpha$  radiation (1.79 Å). Small-angle X-ray scattering (SAXS) patterns were recorded on a Bruker Nanostar U diffractometer using Cu K $\alpha$  radiation (1.54 Å) with a sample to detector distance of 107 cm. Nitrogen physisorption data was obtained on a Quantachrome Autosorb-1 analyzer at 77 K. Thermogravimetric analysis (TGA) was performed using a Seiko Instruments SSC 5200 TG/DTA 220 under O<sub>2</sub> flow. Elemental analyses by inductively coupled plasma atomic emission spectroscopy (ICP-AES) were conducted at Galbraith Laboratories, Inc. (Knoxville, TN.).

Selective gas adsorption measurements were conducted in a Pyrex volumetric apparatus pumped by a liquid nitrogen cooled diffusion pump to sample cell pressures of  $\leq 3 \times 10^{-6}$  torr. The amount of adsorbed gas was measured with a digital pressure gauge (MKS Instruments, PDR-D). Total and reversible isotherms were collected at room temperature with an interim 1 h evacuation between isotherms. Monolayer uptakes were determined by extrapolating adsorbate uptakes to zero pressure ( $P = 0$ ). Catalysts were reduced for 75 min at 673 K in 50 cm<sup>3</sup> (STP) H<sub>2</sub> min<sup>-1</sup> (Praxair, UHP, 99.999%) followed by evacuation at 623 K before adsorption measurements. He (Praxair, UHP, 99.999%), O<sub>2</sub> (Airgas, UHP, 99.999%), and CO (Matheson, UHP, Al cylinder) were all used without further purification. Hemispherical particle sizes were determined from  $d$  (nm) = 1.13/ $D$ , where  $D$  is the metallic dispersion assuming a Pt surface atom density of  $1.27 \times 10^{15}$  cm<sup>-2</sup>.<sup>32</sup>

**2.3.2. Diffuse Reflectance Infrared Study of CO Adsorption on Pt/SBA-15 Catalysts.** In situ diffuse reflectance infrared Fourier

transform spectroscopy (DRIFTS) was used to study the adsorption of CO on various silica supported Pt catalysts. Experiments were conducted with a Nicolet Nexus 670 spectrometer equipped with a Thermo Spectra-Tech controlled atmosphere-diffuse reflection cell. A prereduced Pt/SiO<sub>2</sub> catalyst (ca. 10–40 mg) was loaded in the diffuse reflectance cell and given an abbreviated pretreatment identical to those used for chemisorption and catalytic studies. A single-beam spectrum of the freshly reduced catalyst was obtained at 300 K under 30 cm<sup>3</sup> (STP) He min<sup>-1</sup> and used as the background for spectra of the same catalyst in the presence and absence of gas-phase CO at 300 K. Samples were exposed to a 30 cm<sup>3</sup> (STP) min<sup>-1</sup> flowing mixture of 10% CO/He for 30 min at 300 K, followed by purging in 30 cm<sup>3</sup> (STP) He min<sup>-1</sup> at 300 K. Single-beam scans with a resolution of 2 cm<sup>-1</sup> and a scan number of 128 were collected in the presence and absence of gas-phase CO. The contribution of gas-phase CO was subtracted out of each spectrum with a single-beam spectrum of 10% CO/He measured over a Au mirror. The contribution of adsorbed CO associated with SBA-15 at room temperature was removed by spectral subtraction.

**2.3.3. Catalytic Reaction Measurements.** Catalytic rate measurements were conducted in a plug flow reactor made of Pyrex. Mass flow rates of ethylene (AirGas, CP grade), ethane (Praxair, 99%), hydrogen (Praxair, UHP, 99.999%), and He (Praxair, UHP, 99.999%) were controlled by mass flow controllers (Unit Instruments). Reaction temperatures were measured with a thermocouple extending into the catalyst bed. Reactants and products were detected by gas chromatography (Hewlett-Packard 5890 Series II) and quantified using Dietz tables.<sup>33</sup> Rate measurements for both ethylene hydrogenation and ethane hydrogenolysis were conducted at differential conditions (all conversions,  $X < 10\%$ ). Typically, catalysts (2–300 mg) were diluted with low surface area acid washed quartz in a 1:3 (catalyst/quartz) ratio. Dilution ratios of up to 10 had no effect on the observed conversion. All rates were verified free of heat and mass transfer limitations.

## 3. Results and Discussion

**3.1. Encapsulation of Pt Nanoparticles by SBA-15 and a Plausible Mechanism for Catalyst Formation.** It was determined that upon addition of PVP-capped Pt nanoparticles to the acidic conditions of SBA-15 synthesis, Pt nanoparticles aggregated and the silica matrices were disordered<sup>20,21</sup> (see the Supporting Information). For this reason, SBA-15 was synthesized under neutral conditions using sodium fluoride and a different organosilicon source, tetramethyl orthosilicate (TMOS). PVP-capped Pt particles with sizes of 1.7, 2.9, 3.6, and 7.1 nm were introduced into the neutral pH reaction mixture. In a typical reaction, Pt colloidal solution was mixed with aqueous polymer solution at 313 K and stirred for 1 h to ensure complete dissolution of Pt particles. Brown precipitates were formed 5 min after the addition of NaF solution and TMOS. The supernatant was colorless and transparent, indicating that all Pt colloids were incorporated into the silica matrix. The slurry was aged for a day at 313 K and placed in an oven at 373 K for an additional day. The product was washed with water and ethanol and dried in air at 373 K. Pt/SBA-15 catalysts were obtained by calcination of the raw materials under optimal conditions (vide infra). Figure 1 shows that the Pt nanoparticles are encapsulated by ordered silica structures and the Pt particles are isolated and randomly distributed throughout the entire silica framework without severe agglomeration.

Free PVP is very hydrophilic because of the polar pyrrolidone functionality attached to the main alkyl chain. It dissolves in water, ethanol, and chloroform, while PVP-capped Pt nano-

(25) Singh, U. K.; Vannice, M. A. *J. Catal.* **2000**, *191*, 165.

(26) Bond, G. C.; Wells, P. B. *Appl. Catal.* **1985**, *18*, 221.

(27) Bond, G. C.; Wells, P. B. *Appl. Catal.* **1985**, *18*, 225.

(28) Geus, J. W.; Wells, P. B. *Appl. Catal.* **1985**, *18*, 231.

(29) Frennet, A.; Wells, P. B. *Appl. Catal.* **1985**, *18*, 243.

(30) Wells, P. B. *Appl. Catal.* **1985**, *18*, 259.

(31) Song, H.; Kim, F.; Connor, S.; Somorjai, G. A.; Yang, P. *J. Phys. Chem. B* **2005**, *109*, 188.

(32) Anderson, J. R. *Structure of Metallic Catalysts*; Academic Press: New York, 1975.

(33) Dietz, W. A. *J. Gas Chromatogr.* **1967**, *5*, 68.

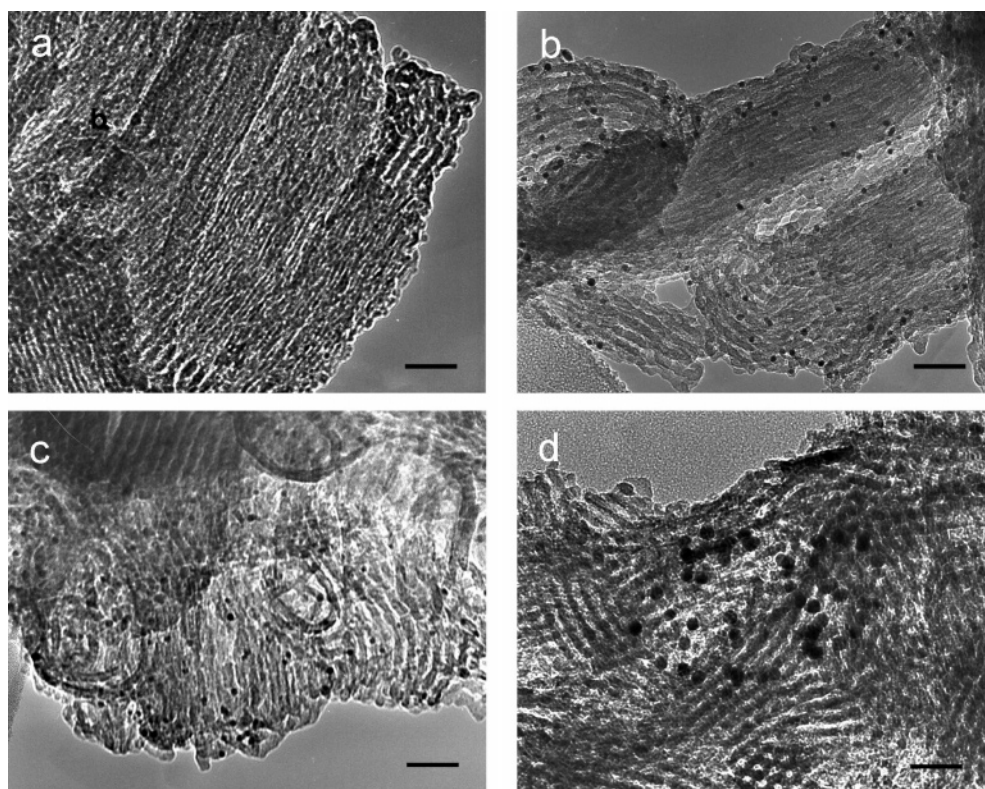


**Figure 1.** TEM images of Pt(X)/SBA-15 catalysts. X = (a) 1.7 nm, (b) 2.9 nm, (c) 3.6 nm, and (d) 7.1 nm. The scale bars represent 40 nm.

**Table 1.** Water Contact Angle of Polymers (PVP and Pluronic P123) and Pt Nanoparticles

Si substrate	$\theta_{\text{H}_2\text{O}}$ (deg)
bare Si substrate	52
PVP layer	15
PVP-capped Pt layer	39
PVP-capped Pt LB layer	53
Pluronic P123 layer	26

particles are poorly soluble in water. The addition of Pluronic P123 helps to form a stable colloidal solution of Pt nanoparticles in water. Water contact angles have been measured to check the hydrophilicity of materials used during catalyst synthesis (Table 1). A PVP layer on the Si substrate exhibits a contact angle of 15°, the lowest value in Table 1 and therefore the most hydrophilic. PVP-capped Pt nanoparticle layers made by drop casting and Langmuir–Blodgett techniques<sup>31</sup> are relatively hydrophobic with contact angles of 39° and 53°, respectively. The more hydrophobic nature of the PVP-capped Pt nanoparticle layers is due to the strong interaction between the pyrrolidone rings of PVP and Pt, resulting in the exposure of the hydrophobic main chain at the surface. Pluronic P123 is known to form spherical micelles in water at room temperature, with the hydrophobic propylene oxide unit in the core and the hydrophilic ethylene oxide unit comprising the sphere surface.<sup>34</sup> Therefore, PVP-capped Pt nanoparticles are likely to be encapsulated within the core of Pluronic P123 micelles. After NaF and TMOS are added to the reaction mixture, silica species polymerize on the surface of Pluronic P123 micelles, and the final product contains Pt particles inside the mesoporous framework. The separate formation of SBA-15 with Pluronic P123 and adsorption of the

**Table 2.** Elemental Analysis and Physisorption Data on Pt-loaded SBA-15

support/catalyst <sup>a, b, c</sup>	N <sub>2</sub> BET parameters		
	surface area (m <sup>2</sup> g <sup>-1</sup> )	pore vol cc(STP) g <sup>-1</sup>	pore diameter (Å) <sup>d</sup>
SBA-15 prepared in acidic conditions <sup>e</sup>	765	1.16	90
SBA-15 prepared in neutral conditions	619	2.05	113
0.6% Pt(1.7 nm)/SBA-15	661	1.58	112
0.77% Pt(2.9 nm)/SBA-15	567	1.50	113
0.6% Pt(3.6 nm)/SBA-15	523	1.42	113
0.62% Pt(7.1 nm)/SBA-15	545	1.65	113

<sup>a</sup> Actual metal loading determined by ICP-AES. <sup>b</sup> Particle sizes measured from XRD data of free-standing Pt colloidal particles. <sup>c</sup> SBA-15 synthesized in neutral conditions. <sup>d</sup> Determined from the adsorption branch of the N<sub>2</sub> isotherm. <sup>e</sup> From ref 18.

Pt particles on its surface cannot be excluded, but the enhanced solubility of PVP-capped Pt nanoparticles in a Pluronic solution suggests that Pt quickly associates with the Pluronic upon its introduction to the solution.

**3.2. Characterization of Pt/SBA-15 Catalysts. 3.2.1. Physical Characterization of Pt/SBA-15 Catalysts.** The resulting SBA-15 and Pt(X)/SBA-15 catalysts (X = 1.7, 2.9, 3.6, and 7.1 nm) were characterized by elemental analysis, XRD, and SAXS. Catalysts were prepared with a nominal weight loading of 1%; actual metal loadings determined by elemental analysis were between 0.6 and 0.8 wt % (Table 2). Three characteristic peaks for Pt(7.1 nm)/SBA-15 appear in the XRD spectra (Figure 2A) at  $2\theta = 45.9^\circ$ ,  $54.0^\circ$ , and  $80.1^\circ$  corresponding to the (111), (200), (220) reflections of the Pt fcc lattice, respectively, as well as a broad amorphous SiO<sub>2</sub> signal at  $2\theta = 27.4^\circ$ . Estimation of the particle size based on XRD was not successful because of the low signal-to-noise ratio of the peaks, except in the case of

(34) Alexandridis, P.; Holzwarth, J. F.; Hatton, T. A. *Macromolecules* **1994**, *27*, 2414.

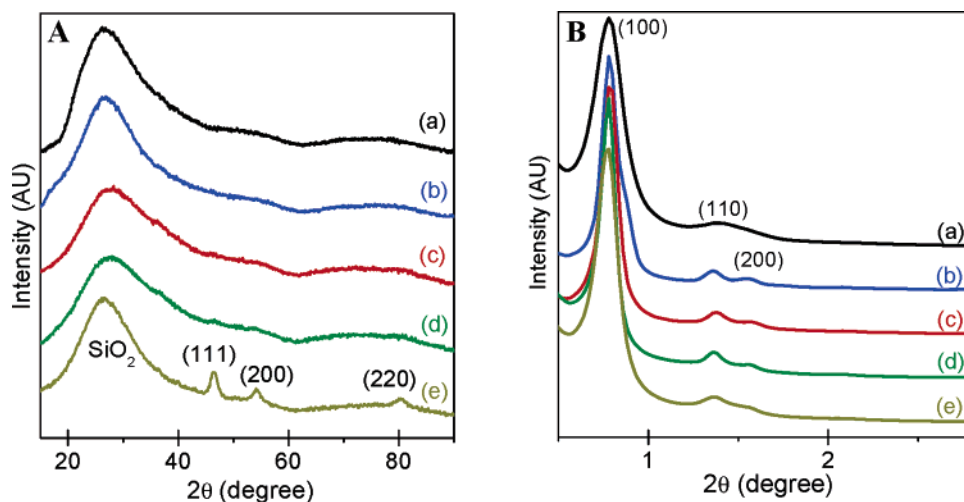


**Figure 2.** (A) XRD data for (a) SBA-15 and Pt(X)/SBA-15 catalysts.  $X =$  (b) 1.7 nm, (c) 2.9 nm, (d) 3.6 nm, and (e) 7.1 nm. The Pt(111), Pt(110), and Pt(200) peaks of the fcc lattice are indicated for Pt(7.1 nm)/SBA-15. Spectra are offset for clarity. (B) SAXS data for (a) SBA-15 and Pt(X)/SBA-15 catalysts.  $X =$  (b) 1.7 nm, (c) 2.9 nm, (d) 3.6 nm, and (e) 7.1 nm. The SBA-15(100), (110), and (200) peaks are indicated, demonstrating the long-range order of the channels. Spectra are offset for clarity.

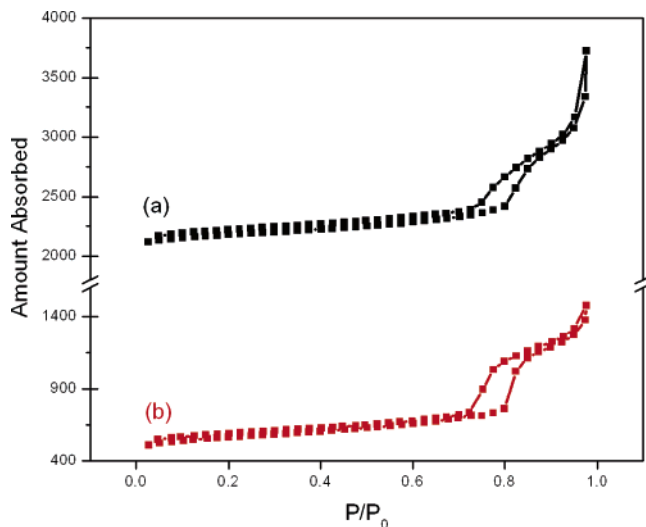


**Figure 3.**  $N_2$  adsorption-desorption isotherms of (a) SBA-15 and (b) 0.77% Pt(2.9 nm)/SBA-15 catalysts. Isotherms for the other catalysts look similar and are therefore not included. The hysteresis loop observed is indicative of cylindrical pores. Isotherms are offset for clarity.

Pt(7.1 nm)/SBA-15. SAXS data (Figure 2B) exhibit three peaks assignable to (100), (110), and (200) of the hexagonal mesostructure with the same  $p6mm$  symmetry as observed in pristine SBA-15.<sup>17</sup> Pt/SBA-15 catalysts exhibit relatively strong (110) and (200) peaks compared to those of SBA-15 in neutral conditions, suggesting that the presence of PVP-capped Pt nanoparticles enhances the ordering of the polymer's hexagonal structure during reaction. Lattice spacings of  $d_{100}$  are almost constant ( $\sim 11$  nm) with variation in particle size, in contrast to previous results of Somorjai and co-workers,<sup>20,21</sup> in which the lattice parameter of Au/SBA-15 increased with the incorporation of larger Au nanoparticles into the mesoporous structure.

BET  $N_2$  adsorption measurements were carried out on the Pt/SBA-15 catalysts (Figure 3). Surface areas of the catalysts ranged from 523 to 661  $m^2 g^{-1}$ ; comparable to pristine SBA-15 (Table 2).<sup>17</sup> Average pore diameters calculated from adsorption branches are  $\sim 11$  nm, and pore volumes determined by the Kelvin equation at  $P/P_0 = 0.975$  are  $\sim 1.42$ – $2.05$   $cm^3$  (STP)  $g^{-1}$ , which are larger than the pore volume of SBA-15

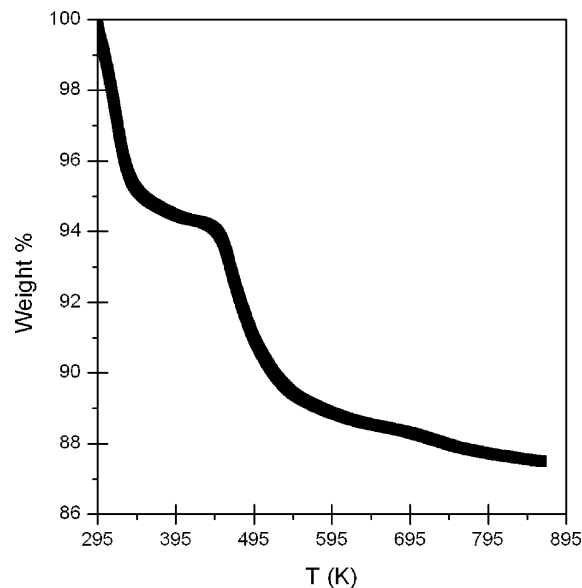


**Figure 4.** TGA data of the as-synthesized 0.77% Pt(2.9 nm)/SBA-15 under a continuous  $O_2$  flow. Three weight loss regimes are observed. The first step is attributed to loss of water, the second to decomposition of Pluronic P123, and the third to decomposition of PVP.

synthesized in acidic conditions (see Table 2 and the Supporting Information).

Removal of PVP while maintaining nanoparticle dispersion represents a significant challenge. Technical catalysts are typically activated by thermal treatment in an inert atmosphere or oxygen followed by reduction to produce a clean, reduced catalyst. Previous work demonstrated that Pt-PVP covered nanoparticles deposited into calcined SBA-15 by sonication required calcination times between 12 and 24 h and temperatures  $\geq 573$  K for PVP removal.<sup>18</sup> In the case of nanoparticle encapsulation catalysts prepared here, three distinct weight loss regimes are evident from thermogravimetric analysis (TGA) of as-synthesized 0.77% Pt(2.9 nm)/SBA-15 sample (Figure 4). Water desorbed below 373 K, Pluronic P123 decomposed at 453–573 K, and PVP decomposed at 573–773 K under  $O_2$ . On the basis of this information, Pt/SBA-15 catalysts were treated with 50  $cm^3$  (STP)  $O_2$   $min^{-1}$  at 723 K for 24–36 h.

**Table 3.** Selective Gas Uptakes and Pt Particle Sizes for Supported Pt/Silica Catalysts

catalyst <sup>a</sup>	selective gas uptake ( $\mu\text{mol g}^{-1}$ ) <sup>b</sup>					dispersion, $D^c$	particle size, $d$ (nm)	
	$\text{H}_2$ , total	$\text{CO}$ , total	$\text{CO}$ , irr	$\text{O}_2$ , irr	$\text{H}_2$ – $\text{O}_2$ , total		chemisorption <sup>d</sup>	XRD
3.2% Pt/SiO <sub>2</sub> –IE	133.1	166.7	152.2	24.2	262.0	1 <sup>e</sup>	1.0	
6.3% Pt/SiO <sub>2</sub> (EUROPT-1)	151.2	182.0	175.0	94.6	334.0	0.69	1.6	1.8 <sup>f</sup>
0.6% Pt(1.7 nm)/SBA-15	4.5	13.3	12.0	4.4	19.1	0.41	2.7	
0.77% Pt(2.9 nm)/SBA-15	6.0	11.3	10.0	4.4	21.8	0.36	3.1	
0.6% Pt(3.6 nm)/SBA-15	4.0	7.9	7.4	3.1	12.5	0.27	4.2	
0.62% Pt(7.1 nm)/SBA-15	2.0	3.4	3.2	2.4	5.6	0.11	9.5	7.9 <sup>g</sup>
Pt powder	16.7	15.1	13.7	8.6	30.3	0.004	287	>100

<sup>a</sup> Actual catalyst loading determined by ICP-AES. <sup>b</sup> Monolayer uptakes ( $P = 0$ ) determined at 295 K. <sup>c</sup> Based on total  $\text{H}_2$ – $\text{O}_2$  titration uptake at  $P = 0$ . <sup>d</sup> Based on  $d$  (nm) =  $1.13/D$ . <sup>e</sup> Dispersion greater than unity calculated; assumed 100% dispersion for calculation of turnover frequency. <sup>f</sup> From Gnutzman, V.; Vogel, W. *J. Phys. Chem.* **1990**, *94*, 4991. <sup>g</sup> After subtraction of pristine SBA-15 background.

The Pt(1.7 nm)/SBA-15 was treated at 623 K for 24 h in order to prevent severe agglomeration of the particles. Chandler and co-workers obtained similar results for dendrimer covered Pt nanoparticles; dendrimer was effectively removed for nanoparticles deposited directly on a silica support,<sup>35</sup> while the same calcination–reduction procedure was ineffective for dendrimer removal from nanoparticles encapsulated during synthesis of a microporous xerogel silica.<sup>36</sup> The stage at which the dendrimer covered nanoparticles were introduced into the xerogel synthesis had an influence on the degree of poisoning; addition of particles after sol formation were poisoned to a greater extent by dendrimer decomposition products than nanoparticles added before sol formation. Chandler and co-workers<sup>36</sup> suggest that the small pores ( $\leq 2$  nm) of the xerogel inhibit transport of dendrimer decomposition products from the nanoparticle surface. In the case of the nanoparticle encapsulation method, nanoparticles are added before sol formation, and it is proposed that some of the Pt may be occluded in silica capsules which can form during SBA-15 synthesis,<sup>37</sup> although capsules have not been observed in our microscopy studies. Chemical titration of the metal surface area has proven that most of the nanoparticle surface area is accessible for adsorption and reaction.

**3.2.2. Particle Size Determination by Chemisorption.** Particle size measurements by TEM and XRD verified that particle size was not perturbed during the nanoparticle encapsulation synthesis. Particle sizes obtained from these measurements are not a good measure of the catalytically relevant particle size. Before calcination, the nanoparticle surfaces contain the surface-regulating agent, PVP, which bonds very strongly to the Pt surface. Removal of this polymer requires high temperature as shown by thermogravimetric analysis (TGA) (Figure 4), and care must be taken to ensure sufficient polymer removal without severe sintering. Selective adsorption of probe gases represents the most appropriate probe for determining Pt particle size and is used to normalize measured reaction rates to the exposed metal surface area.<sup>38</sup> Chemisorption is sensitive to the polymer presence on the nanoparticle surface and any changes in particle size during pretreatment. Particle size was determined by chemisorption with three independent measurements,  $\text{H}_2$ , CO, and  $\text{H}_2$ – $\text{O}_2$  titration. Adsorption uptakes and particle sizes calculated assuming hemispherical particle

geometry are compiled in Table 3. The three independent techniques are in relatively good agreement, and variance in particle size determined by the different adsorption techniques may be a consequence of changes in adsorbate stoichiometry with particle size or the influence of residual PVP on the nanoparticle surface. Regardless, the agreement with TEM measurements and XRD (except in the case of Pt(7.1 nm)/SBA-15) is very good. Measured dispersion for the two reference catalysts are in good agreement with previously reported results. Catalytic activities are normalized per surface atom based on total  $\text{H}_2$ – $\text{O}_2$  titration uptake.

**3.2.3. Infrared Spectroscopic Measurements of CO Adsorption.** The adsorption of carbon monoxide has been used as a probe of local surface structure, both geometric and electronic.<sup>39,40</sup> The geometry in which CO bonds to the surface, the position of such vibrations in the infrared region, and the line shape of the absorption band are qualitative probes of Pt surface structure. An example of the sensitivity of CO adsorption to surface site coordination is the adsorption of CO on low-index surfaces (Pt(111)) and stepped Pt surfaces (Pt(211)). The stretching frequency of adsorbed CO on Pt(111) is 2090–2100  $\text{cm}^{-1}$  at high coverages.<sup>41</sup> Upon the introduction of coordinatively unsaturated atoms onto Pt single-crystal surfaces, atop adsorption of CO on terrace ( $\sim 2090$   $\text{cm}^{-1}$ ) and step ( $\sim 2075$   $\text{cm}^{-1}$ ) sites can be distinguished at low temperatures ( $\sim 100$  K), but at higher temperatures, as employed in this study, distinction between the two adsorbate–surface site interactions is more difficult, likely due to facile surface diffusion between the two sites.<sup>42</sup>

The influence of particle size on CO adsorption was examined in this work. Infrared spectra (1900–2200  $\text{cm}^{-1}$ ) demonstrate that atop-bonded CO is the dominant interaction between CO and the Pt surface. No bridge-bonded CO was observed on any catalyst used in this study, though it has been previously observed on Pt/SiO<sub>2</sub>. Figure 5 demonstrates the position of the atop frequency red-shifted by  $\sim 15$   $\text{cm}^{-1}$  between the 1.7 and 7.1 nm particles. The clear distinction between particle sizes confirms that CO is a good probe molecule for assessing the state of the Pt surface. Cant and Donaldson<sup>43</sup> have shown a minor influence of particle size on the position of the atop CO vibration for two Pt/SiO<sub>2</sub> catalysts with surface average particle

- (35) Lang, H.; May, R. A.; Iverson, B. L.; Chandler, B. D. *J. Am. Chem. Soc.* **2003**, *125*, 14832.  
 (36) Beakley, L. W.; Yost, S. E.; Cheng, R.; Chandler, B. D. *Appl. Catal., A* **2005**, *292*, 124.  
 (37) Van Der Voort, P.; Ravikovitch, P. I.; De Jong, K. P.; Benjelloun, M.; Van Bavel, E.; Janssen, A. H.; Neimark, A. V.; Weckhuysen, B. M.; Vansant, E. F. *J. Phys. Chem. B* **2002**, *106*, 5873.  
 (38) Boudart, M. *Adv. Catal.* **1969**, *20*, 153.

- (39) Little, L. H. *Infrared Spectra of Adsorbed Species*; Academic Press: New York, 1966.  
 (40) Hair, M. L. *Infrared Spectroscopy in Surface Chemistry*; Dekker: New York, 1967.  
 (41) McCrea, K. R.; Parker, J. S.; Chen, P. L.; Somorjai, G. A. *Surf. Sci.* **2001**, *494*, 238.  
 (42) Mukerji, R. J.; Bolina, A. S.; Brown, W. A. *Surf. Sci.* **2003**, *527*, 198.  
 (43) Cant, N. W.; Donaldson, R. A. *J. Catal.* **1982**, *78*, 461.

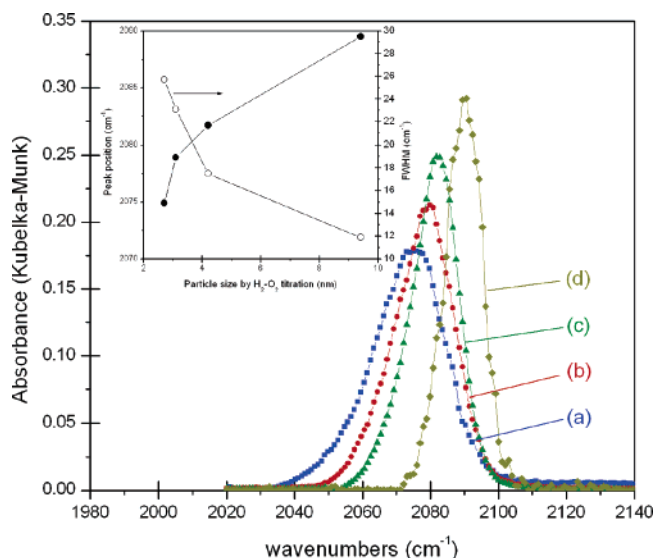


**Figure 5.** Infrared spectrum of CO adsorption at 295 K for the Pt/SBA-15 catalyst series: (a) 2.33% Pt(1.7 nm)/SBA-15, (b) 2.69% Pt(2.9 nm)/SBA-15, (c) 2.62% Pt(3.6 nm)/SBA-15, and (d) 2.86% Pt(7.1 nm)/SBA-15. Inset is the peak position and fwhm of the atop CO stretching vibration as a function of particle size at room temperature. At saturation coverage, the peak position red-shifts due to changes in the average coordination number as the particle decreases. Peak heights have been modified for clarity.

sizes as determined by  $H_2$  chemisorption of 1.8 and 18 nm; the band position for the 1.8 nm was red-shifted by  $6\text{ cm}^{-1}$  relative to the 18 nm Pt particle silica catalyst ( $2078\text{ cm}^{-1}$ ). Bischoff et al.<sup>44</sup> have studied the effect of particle size on CO adsorption for Pt dispersed within a neutralized faujasite zeolite. The authors suggest that a clear particle size dependent shift of the atop adsorbed CO stretching vibration was observed due to the narrow Pt particle size distribution. At room temperature, the absorption of the atop CO stretching frequency was at  $\sim 2050\text{ cm}^{-1}$  for 1–2 nm particles and  $\sim 2100\text{ cm}^{-1}$  for 4–5 nm particles. Clearly, work on single crystals<sup>41,42</sup> and supported catalysts<sup>43,44</sup> suggest that the position of the atop CO vibration red-shifts with increasing surface roughness and decreasing particle size. The stretching frequency of a single CO molecule on a  $Pt_{10}$  cluster as determined by DFT calculations is  $2050\text{ cm}^{-1}$ ,<sup>45</sup> while a single CO stretching vibrational frequency of  $2020\text{ cm}^{-1}$  was reported for gas-phase CO saturated neutral  $Pt_3(CO)_6$  clusters.<sup>46</sup> Vibrational frequencies for atop CO have been reported as low as  $2000\text{ cm}^{-1}$  for  $Pt(CO)_2$ -type surface species.<sup>47</sup> The work presented here is in agreement with previous studies and suggests that the strength of  $\pi$  back-donation of the CO chemisorption bond is stronger on a small particle with a larger fraction of low-coordination metal sites relative to that of a single crystal or platinum particle with a large fraction of high-coordination surface sites.<sup>47</sup>

The inset of Figure 5 demonstrates that the full width at half-maximum (fwhm) increases as the nanoparticle size decreases. Although these spectra have a narrower fwhm than that of a conventional catalyst due to their monodisperse particles, within the series of Pt/SBA-15 catalysts, the decrease in fwhm as the

**Table 4.** Ethylene Hydrogenation Turnover Rates and Kinetic Parameters on Pt Catalysts

catalyst <sup>a</sup>	activity ( $\mu\text{mol g}^{-1}\text{ s}^{-1}$ ) <sup>b</sup>	TOF ( $\text{s}^{-1}$ ) <sup>b,c</sup>	$E_a$ ( $\text{kcal mol}^{-1}$ ) <sup>d</sup>	reaction orders	
				$C_2H_4$ <sup>e</sup>	$H_2$ <sup>f</sup>
3.2% Pt/SiO <sub>2</sub> -IE	623	3.8	8.0	-0.1	0.62
0.6% Pt(1.7 nm)/SBA-15	45	3.5	10.5	0	0.57
0.77% Pt(2.9 nm)/SBA-15	50	3.5	9.8	0	0.48
0.6% Pt(3.6 nm)/SBA-15	28	3.4	10.1	0.1	0.47
0.62% Pt(7.1 nm)/SBA-15	11	3.2	12.1	0.1	0.51
Pt powder	69	3.4	8.9	-0.1	0.4

<sup>a</sup> Actual catalyst loading determined by ICP-AES. <sup>b</sup> Initial activity. Reaction conditions were 10 torr  $C_2H_4$ , 100 torr  $H_2$ , and 298 K. <sup>c</sup> Normalized to the number of surface atoms determined by total  $H_2-O_2$  titration. <sup>d</sup> Reaction conditions were 10 torr  $C_2H_4$ , 200 torr  $H_2$ , and 273–323 K. <sup>e</sup> Reaction conditions were 10–40 torr  $C_2H_4$ , 200 torr  $H_2$ , and 298 K. <sup>f</sup> Reaction conditions were 10 torr  $C_2H_4$ , 200–600 torr  $H_2$ , and 298 K.

particle size increases suggests that on the larger particles there is less surface heterogeneity because the surface is terminated by large terraces of identical surface atoms. As the nanoparticle size decreases, the surface heterogeneity increases due to changing surface atom statistics<sup>48</sup> and the infrared spectrum represents an ensemble average of CO vibrations on all sites resulting in a broadened peak. In a similar study, Lang et al.<sup>35</sup> demonstrated that fwhm for adsorbed CO on dendrimer-templated nanoparticles supported on  $SiO_2$  was much narrower as compared to that of a Pt catalyst synthesized by incipient wetness on the same silica because of a much narrower TEM particle size distribution for the dendrimer particles ( $\sigma = 20\%$ ) as compared to that of the standard Pt catalyst ( $\sigma = 50\%$ ). The infrared data on dendrimer-derived Pt nanoparticles is similar to that found in this study.

### 3.3. Catalytic Rate Measurements of Hydrocarbon Conversion Reactions. 3.3.1. Ethylene Hydrogenation.

Ethylene hydrogenation was chosen as a probe reaction to assess the extent of polymer removal and to compare the activity of nanoparticle encapsulation catalysts with classically prepared supported catalysts and single crystals. The insensitivity of catalytic activity and kinetic parameters to Pt particle size and surface structure is well-known for this reaction.<sup>49</sup> Specific activities and turnover frequencies at standard conditions of 10 torr  $C_2H_4$ , 100 torr  $H_2$ , and 298 K are reported in Table 4. At standard conditions, all catalysts have initial turnover frequencies of  $\sim 3.5\text{ s}^{-1}$ , in good agreement with the room-temperature turnover frequency of  $10\text{ s}^{-1}$  on a Pt(111) single crystal under similar pressure conditions.<sup>50</sup> At similar conditions, turnover frequencies as high as  $20\text{ s}^{-1}$ <sup>51</sup> and as low as  $3 \times 10^{-3}\text{ s}^{-1}$ <sup>52</sup> have been measured on  $SiO_2$  supported Pt catalysts. Figure 6 demonstrates the influence of particle size on catalytic activity with time on stream. Initial rates (Table 4) are identical, but steady-state rates (after 40 ks) decrease with increasing particle size. The reason for this behavior is unknown at the time but may be related to stronger adsorption of ethylidyne and its subsequent decomposition on the surface of larger particles. Comparison of the initial heats of adsorption of ethylene and identification of adsorbed species by various surface spectroscopy suggests that the dehydrogenation of adsorbed ethylene is suppressed on small crystallites.<sup>53,54</sup> Paul et al.<sup>55</sup> have shown

(44) Bischoff, H.; Jaeger, N. I.; Schulz-Ekloff, G. *Z. Phys. Chem. (Leipzig)* **1990**, *271*, S1093.

(45) Watwe, R. M.; Spiewak, B. E.; Cortright, R. D.; Dumesic, J. A. *Catal. Lett.* **1998**, *51*, 139.

(46) Schulze Icking-Konert, G.; Handschuh, H.; Ganteför, G.; Eberhardt, W. *Phys. Rev. Lett.* **1996**, *76*, 1047.

(47) Härle, H.; Metka, W.; Volpp, H.-R.; Wolfrum, J. *Phys. Chem. Chem. Phys.* **1999**, *1*, 5059.

(48) Van Hardeveld, R. V.; Hartog, F. *Surf. Sci.* **1969**, *15*, 189.

(49) Dorling, T. A.; Eastlake, M. J.; Moss, R. L. *J. Catal.* **1969**, *14*, 23.

(50) Zaera, F.; Somorjai, G. A. *J. Am. Chem. Soc.* **1984**, *106*, 2288.

(51) Schlatter, J. C.; Boudart, M. *J. Catal.* **1972**, *24*, 482.

(52) Sinfelt, J. H. *J. Phys. Chem.* **1964**, *68*, 856.

(53) Gay, I. D. *J. Catal.* **1987**, *108*, 15.

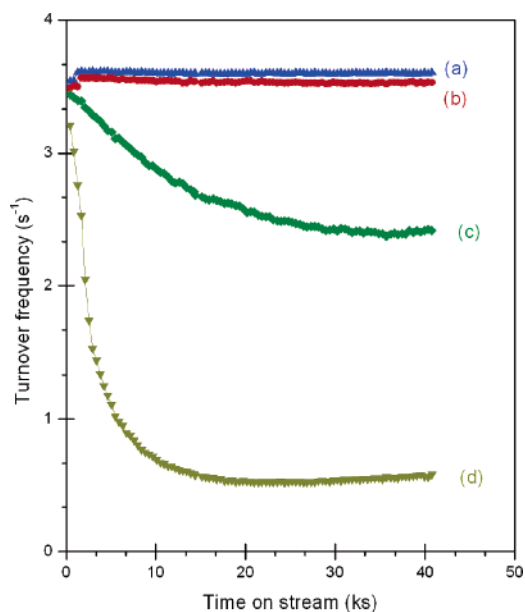


**Figure 6.** Time on stream behavior during ethylene hydrogenation on Pt(X)/SBA-15 catalyst. X = (a) 1.7 nm, (b) 2.9 nm, (c) 3.6 nm, and (d) 7.1 nm. Reaction conditions were 10 torr C<sub>2</sub>H<sub>4</sub>, 100 torr H<sub>2</sub>, and 298 K. Turnover frequencies were calculated from metal dispersions determined by H<sub>2</sub>-O<sub>2</sub> titration. All catalysts have the same initial turnover frequency, but the catalysts with larger metal particles deactivate with time on stream.

by vibrational coupling that ethylidyne is produced on (111) facets of small Pt particles ( $d = 10\text{--}40 \text{ \AA}$ , ave  $20 \text{ \AA}$ ) rather than on random trimer Pt sites and no ethylidyne was detected on highly dispersed Pt particles ( $d \leq 10 \text{ \AA}$ ). Passos et al.<sup>56</sup> found that the initial heat of adsorption at 300 K was  $10 \text{ kcal mol}^{-1}$  higher on large ( $\sim 20 \text{ nm}$ ) Pt particles as compared with that on small Pt particles ( $\sim 1 \text{ nm}$ ); the higher heat of adsorption on large crystals is attributed to the exothermic dehydrogenation of ethylene to ethylidyne or ethylidene.<sup>57</sup> These surface reactions are not probed by UHV temperature-programmed desorption (TPD) from Pt single-crystal surfaces because only the desorption of reversibly adsorbed molecular C<sub>2</sub>H<sub>4</sub> is measured. Correction of reported TPD data for the enthalpy of reaction for the dehydrogenation of ethylene to ethylidyne yields ethylene heat of adsorption values on Pt single crystals which are similar to values measured on large ( $\geq 4 \text{ nm}$ ) Pt crystallites.<sup>56,58</sup>

The increased heat of adsorption of ethylene on larger crystallites suggests that the barrier for ethylidyne surface diffusion may be higher on larger crystallites, although extended Hückel calculations of C<sub>2</sub>H<sub>3</sub> surface diffusion on Pt(111) suggest that the required activation energy is low ( $2.3 \text{ kcal mol}^{-1}$ ).<sup>59</sup> Stronger heats of adsorption should hinder adsorbate mobility, critical for catalytic turnover,<sup>60</sup> and the increased residence time of C-C species on the surface may lead to their decomposition and eventual poisoning until a steady-state carbon coverage is obtained. A model of a supported ethylene hydrogenation catalyst under reaction conditions may be similar to the model proposed for a Pt reforming catalyst.<sup>61</sup>

**Table 5.** Ethane Hydrogenolysis Turnover Rates and Kinetic Parameters on Pt Catalysts

catalyst <sup>a</sup>	activity ( $\mu\text{mol g}^{-1} \text{ s}^{-1}$ ) <sup>b</sup>	TOF $100 \times (\text{s}^{-1})^{\text{b,c}}$	E <sub>a</sub> (kcal mol <sup>-1</sup> ) <sup>d</sup>	reaction orders C <sub>2</sub> H <sub>6</sub> <sup>e</sup>	H <sub>2</sub> <sup>f</sup>
3.2% Pt/SiO <sub>2</sub> -IE	10.6	6.5	54.5	0.99	-2.8
6.3% Pt/SiO <sub>2</sub> (EUROPT-1)	11.3	4.7	46.0	0.9	-1.8
0.6% Pt(1.7 nm)/SBA-15	0.16	1.2	63.4	0.97	-2.4
0.77% Pt(2.9 nm)/SBA-15	$7.8 \times 10^{-2}$	0.6	68.7	1	-3.1
0.6% Pt(3.6 nm)/SBA-15	$1.1 \times 10^{-2}$	0.1	75.8	1.1	-3.0
0.62% Pt(7.1 nm)/SBA-15	$6.5 \times 10^{-3}$	0.08	74.5	0.97	-2.9
Pt powder	$7 \times 10^{-3}$	0.04	70.5	0.99	-2.6

<sup>a</sup> Actual catalyst loading determined by ICP-AES. <sup>b</sup> Reaction conditions were 20 torr C<sub>2</sub>H<sub>6</sub>, 200 torr H<sub>2</sub>, and 658 K. <sup>c</sup> Normalized to the number of surface atoms determined by total H<sub>2</sub>-O<sub>2</sub> titration. <sup>d</sup> Reaction conditions were 20 torr C<sub>2</sub>H<sub>6</sub>, 200 torr H<sub>2</sub>, and 593-673 K. <sup>e</sup> Reaction conditions were 10-60 torr C<sub>2</sub>H<sub>6</sub>, 200 torr H<sub>2</sub>, and 658 K. <sup>f</sup> Reaction conditions were 20 torr C<sub>2</sub>H<sub>6</sub>, 140-270 torr H<sub>2</sub>, and 658 K.

Hydrogenation of ethylene is easily catalyzed at room temperature, with apparent activation energies of  $\sim 10 \text{ kcal mol}^{-1}$  for the Pt/SBA-15 catalyst series. One notable exception is the apparent activation energy of  $12 \text{ kcal mol}^{-1}$  for the 0.62% Pt(7.1 nm)/SBA-15 catalyst. Activation energies in this range have been attributed to a dirty or poisoned catalyst surface.<sup>51</sup> During the synthesis of 7.1 nm Pt nanoparticles, 12-fold molar excess of PVP is added relative to the Pt concentration. The larger excess of PVP was removed with a 723 K calcination time of 36 h (2.9 and 3.6 nm particles were calcined at 723 K for 24 h). It is possible that the higher apparent activation energy is due to the presence of residual polymer, although TGA of 7.1 nm particles suggests that PVP decomposes over the same temperature range as that observed on the 2.9 nm particles.<sup>62</sup> The observed time on stream deactivation dependence of Pt(7.1 nm)/SBA-15 may be related to residual PVP on the surface. Partial pressure dependencies of ethylene hydrogenation over encapsulated nanoparticles (Table 4) are in accord with classically prepared samples. Dependence on ethylene and hydrogen partial pressures are  $\sim 0.1$  and  $0.5$ , respectively, for the Pt/SBA-15 catalysts. Similar to other SiO<sub>2</sub> supported Pt catalysts, the hydrogen reaction order approached unity as the temperature was increased and the ethylene order was zero order at temperatures around room temperature.<sup>63</sup>

**3.3.2. Ethane Hydrogenolysis as a Probe of Structure Sensitivity.** The hydrogenolysis of alkanes has been studied extensively because of the well-known sensitivity of hydrogenolysis rates on surface structure.<sup>64,65</sup> As a test of particle surface structure, the hydrogenolysis of ethane was examined over the Pt/SBA-15 catalysts. Table 5 summarizes the kinetic results of ethane hydrogenolysis; as previously reported, ethane hydrogenolysis is very sensitive to particle size, with turnover frequencies varying by at least 2 orders of magnitude for catalysts containing Pt particles from 1 to 7 nm. Apparent reaction orders in ethane and hydrogen were 1 and  $\sim -3$ , respectively, for the Pt/SBA-15 series. The observed reaction orders are in agreement with measurements on other supported Pt catalysts.<sup>66</sup> Measured apparent activation energies increase with decreasing metal dispersion.

(54) Soma, Y. *J. Catal.* **1982**, *75*, 267.

(55) Paul, D. K.; Beebe, T. P.; Uram, K. J.; Yates, J. T. *J. Am. Chem. Soc.* **1992**, *114*, 1949.

(56) Passos, F. B.; Schmal, M.; Vannice, M. A. *J. Catal.* **1996**, *160*, 118.

(57) Carter, E. A.; Koel, B. E. *Surf. Sci.* **1990**, *226*, 339.

(58) Shen, J.; Hill, J. M.; Watwe, R. M.; Spiewak, B. E.; Dumesic, J. A. *J. Phys. Chem. B* **1999**, *103*, 3923.

(59) Nomikou, Z.; Van Hove, M. A.; Somorjai, G. A. *Langmuir* **1996**, *12*, 1251.

(60) Somorjai, G. A. *Nature* **2004**, *430*, 730.

(61) Somorjai, G. A.; Zaera, F. *J. Phys. Chem.* **1982**, *86*, 3070.

(62) Rioux, R. M.; Song, H.; Habas, S.; Grass, M.; Hoefelmeyer, J. D.; Niesz, K.; Yang, P. D.; Somorjai, G. A. *Top. Catal.*, submitted for publication, 2005.

(63) Cortright, R. D.; Goddard, S. A.; Rekoske, J. E.; Dumesic, J. A. *J. Catal.* **1991**, *127*, 342.

(64) Martin, G. A. *J. Catal.* **1979**, *60*, 452.

(65) Carter, J. L.; Cusumano, J. A.; Sinfelt, J. H. *J. Phys. Chem.* **1966**, *70*, 2257.



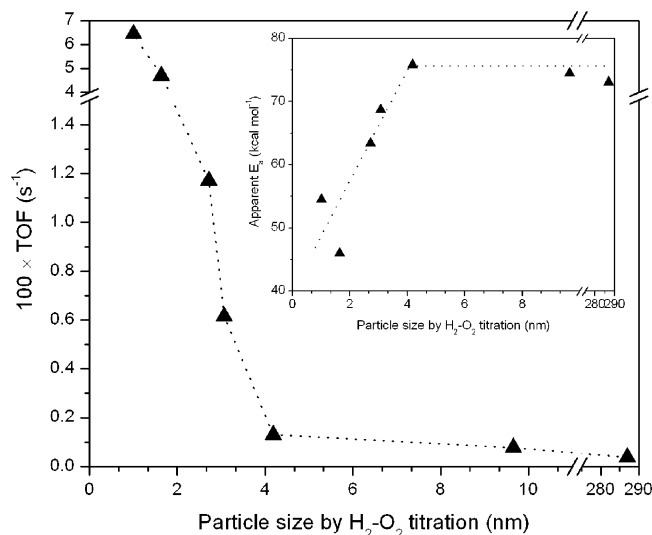


**Figure 7.** Dependence of ethane hydrogenolysis turnover frequency and apparent activation energy on Pt particle size. Turnover frequencies decrease by 2 orders of magnitude over the size range, while the apparent activation energy increases. Coordinatively unsaturated surface atoms in small particles have a higher reactivity and subsequently a smaller barrier for hydrogenolysis than highly coordinated surface atoms of larger particles. Turnover frequencies were measured at 20 torr C<sub>2</sub>H<sub>6</sub>, 200 torr H<sub>2</sub>, and 658 K.

Ion-exchanged 3.2% Pt/SiO<sub>2</sub>-IE with particles of ~1 nm were the most active ( $6.4 \times 10^{-2} \text{ s}^{-1}$  at 658 K) and had an apparent activation energy of 54 kcal mol<sup>-1</sup>. Apparent activation energies increased to ~75 kcal mol<sup>-1</sup> on the 0.6% Pt(3.6 nm)/SBA-15 catalyst. The apparent preexponential factors assuming a power rate law,  $r_{\text{CH}_4} = k_{\text{app}} P_{\text{C}_2\text{H}_6} P_{\text{H}_2}^{-3}$ , where  $k_{\text{app}} = A e^{-E_{\text{app}}/RT}$  varied by 4 orders of magnitude ( $10^{25}$ – $10^{29} \text{ torr}^2 \text{ s}^{-1}$ ) over the particle size range studied. The influence of particle size on catalytic activity and the measured apparent activation energy are shown in Figure 7. As the particle size increases, a linear increase in the apparent activation energy is found, up to a particle size of 3.6 nm, after which the activation energy is unchanged with larger particle size. Figure 7 demonstrates that the turnover frequency for methane formation decreases as the particle size increases; similar trends have been observed on supported Pt catalysts.<sup>67,68</sup> A maximum in ethane hydrogenolysis turnover frequency has been observed for Pt/Al<sub>2</sub>O<sub>3</sub> catalysts with Pt particles ranging from 1.7 to 5 nm.<sup>69</sup> These authors also observe a minimum in the apparent activation energy with particle size; after ~4 nm there is no change in the apparent activation energy. A compilation of reported ethane hydrogenolysis rates normalized to standard conditions of 20 torr C<sub>2</sub>H<sub>6</sub>, 200 torr H<sub>2</sub>, and 658 K is given (see the Supporting Information). Rates of ethane hydrogenolysis follow a trend of decreasing rate with increasing metal particle size on the Pt/SBA-15 series, although significant discrepancies do exist, and these have been highlighted in a recent review.<sup>70</sup> For example, two independent studies of ethane hydrogenolysis on Pt(111) have determined similar turnover frequencies of ~0.3 s<sup>-1</sup> at standard conditions, which is an order of magnitude higher than Pt(1.7 nm)/SBA-15 and 3 orders of magnitude higher than Pt(7.1 nm)/SBA-15.

It is believed that large ensembles of Pt atoms are necessary for ethane hydrogenolysis because the C<sub>2</sub> intermediate is most likely bonded to multiple Pt atoms and adjacent sites are needed for H adsorption. The necessity for a large Pt ensemble is most likely not the only requirement for an appropriate active site for ethane hydrogenolysis. Goodwin et al. suggest that these ensembles must also be properly oriented.<sup>71</sup> Comparison of ethane hydrogenolysis rates on Ni(111) and (100) has led Goodman to suggest that the spatial coordination of surface metal atoms is a decisive factor in determining reactivity; differences in spacing between surface atoms on the two surfaces could account for the differences in activity.<sup>72</sup> The number of atoms in the ensemble varies with metal most likely due to the stoichiometry of the C<sub>2</sub>H<sub>x</sub> species in which the C–C bond is broken. In the case of Ni, methane forms through a surface carbide followed by hydrogen reduction, suggesting that a 12 atom ensemble is required.<sup>73</sup> On Pt, the proposed C<sub>2</sub> intermediate that undergoes C–C bond cleavage on Pt is the ethyl radical, C<sub>2</sub>H<sub>5.<sup>74,75</sup> In this case, the ensemble size may be significantly reduced but the orientation of the atoms composing that ensemble is still critical, most likely requiring a fraction of the ensemble to be composed of atomic steps, kinks, or other sources of surface roughness. Theoretical calculations of C<sub>2</sub>H<sub>x</sub> fragment stability on Pt slabs and clusters have shown that barriers to bond activation are lower on a stepped Pt(211) surface relative to those on a flat (111) surface.<sup>76,77</sup> Correspondingly, the activated complexes along the hydrogenolysis reaction coordinate are stabilized on the stepped surface relative to the flat surface. Small metal crystallites have a higher proportion of coordinatively unsaturated surface atoms, analogous to a stepped single crystal, while the surfaces of large Pt particle are terminated primarily by low-index, high-coordination surfaces. It appears that reactions involving C<sub>2</sub>H<sub>x</sub> and their activated complexes occur on these defect sites because they provide more stable bonding. Recent work has shown that methane activation rates increased with Pt dispersion suggesting that CH<sub>x</sub> species are stabilized on coordinatively unsaturated atoms.<sup>78</sup> The identity of the active site for C–H and C–C bond activation is unknown, but particle size dependent catalytic behavior of ethane hydrogenolysis suggests that surface roughness is a primary component of the active site.</sub>

**3.3.3. Structure Sensitivity of Ethane Decomposition to Surface Carbon during Hydrogenolysis.** Methane is the only product observed in the gas phase, but consideration of the decomposition of ethane to surface carbon as a reaction pathway is an important parameter for the design of hydrogenolysis catalysts. For example, Vang et al.<sup>79</sup> demonstrated that step sites on a Ni single crystal are significantly more reactive for C–C bond breaking than terrace atoms and the selective blocking of

(66) Sinfelt, J. H.; Taylor, W. F.; Yates, D. J. C. *J. Phys. Chem.* **1965**, *68*, 95.  
 (67) Guzzi, L.; Gudkov, B. S. *React. Kinet. Catal. Lett.* **1978**, *9*, 343.  
 (68) Barbier, J.; Morales, A.; Maurel, R. *Bull. Soc. Chim. Fr.* **1978**, 131.  
 (69) Nazimek, D.; Ryczkowski, J. *React. Kinet. Catal. Lett.* **1989**, *40*, 145.  
 (70) Gunter, P. L. J.; Niemandsverdriet, J. W. H.; Ribeiro, F. H.; Somorjai, G. A. *Catal. Rev. Sci. Eng.* **1997**, *39*, 77.

(71) Goodwin, J. G.; Kim, S.; Rhodes, W. D. In *Catalysis*; Spivey, J. J., Ed.; The Royal Society of Chemistry: Cambridge, U.K., 2004; Vol. 17, Chapter 8.  
 (72) Goodman, D. W. *Surf. Sci.* **1982**, *123*, L679.  
 (73) Martin, G. A. *Catal. Rev. Sci. Eng.* **1988**, *30*, 519.  
 (74) Cortright, R. D.; Watwe, R. M.; Spiewak, B. E.; Dumesic, J. A. *Catal. Today* **1999**, *53*, 395.  
 (75) Gudkov, B. S.; Guzzi, L.; Tétényi, P. J. *Catal.* **1982**, *74*, 207.  
 (76) Watwe, R. M.; Spiewak, B. E.; Cortright, R. D.; Dumesic, J. A. *J. Catal.* **1998**, *180*, 184.  
 (77) Watwe, R. M.; Cortright, R. D.; Nørskov, J. K.; Dumesic, J. A. *J. Phys. Chem. B* **2000**, *104*, 2299.  
 (78) Wei, J.; Iglesia, E. *J. Phys. Chem. B* **2004**, *108*, 4094.  
 (79) Vang, R. T.; Honkala, K.; Dahl, S.; Vestergaard, E. K.; Schnadt, J.; Lægsgaard, E.; Clausen, B. S.; Nørskov, J. K.; Besenbacher, F. *Nat. Mater.* **2005**, *4*, 160.

**Table 6.** Exposed Pt Surface Area before and after Ethane Hydrogenolysis on Selected Pt/SBA-15 Catalysts Determined by H<sub>2</sub>-O<sub>2</sub> Titration

catalyst	probe gas uptake ( $\mu\text{mol g}^{-1}$ ) <sup>a</sup>			based on total H <sub>2</sub> -O <sub>2</sub> titration uptake			fraction of Pt surface area exposed
	CO		H <sub>2</sub> -O <sub>2</sub> titr total	dispersion, <i>D</i>	Pt surface area ( $\text{m}^2 \text{g}^{-1}$ ) <sup>b</sup>	Pt particle size (nm) <sup>c</sup>	
	total	irrev					
0.77% Pt(2.9 nm)/SBA-15 before rxn	11.3	10.0	21.8	0.37	14.2	3.1	
0.77% Pt(2.9 nm)/SBA-15 after rxn <sup>d</sup>	8.9	8.9	16.5	0.28	10.7	4.1	0.76
0.77% Pt(2.9 nm)/SBA-15 after calcination <sup>e</sup>	9.4	8.5	21.7	0.37	14.1	3.1	
0.6% Pt(3.6 nm)/SBA-15 before rxn	7.9	7.4	12.5	0.27	8.1	4.2	
0.6% Pt(3.6 nm)/SBA-15 after rxn <sup>d</sup>	6.8	5.6	11.2	0.24	7.3	4.7	0.9
0.6% Pt(3.6 nm)/SBA-15 after calcination <sup>e</sup>	7.5	6.7	12.0	0.26	7.8	4.3	

<sup>a</sup> Measured at 295 K. Monolayer values extrapolated to  $P = 0$ . <sup>b</sup>  $H/Pt = 1$  and cross-sectional area of H<sub>2</sub> molecule =  $10.4 \text{ \AA}^2$  were assumed. <sup>c</sup> Determined by  $d \text{ (nm)} = 1.13/D$ . <sup>d</sup> Measured directly after ethane hydrogenolysis. <sup>e</sup> Sample was calcined for 1 h in 20% O<sub>2</sub>/He at 573 K followed by reduction at 673 K for 1 h.

step sites with inert Au atoms led to a Ni surface capable only of C–H bond activation. In another study, two competing reaction pathways were found for methanol decomposition: C–H bond activation leading to the formation of CO<sub>2</sub> at terrace sites and C–O bond scission leading to carbon covered step sites.<sup>80</sup> In these elegant examples, the morphology and surface roughness of the surface not only influence activity but play an important role in determining reaction selectivity.

The extent of carbon deposited on Pt/SBA-15 after hydrogenolysis has been determined by H<sub>2</sub>-O<sub>2</sub> titration. It has been suggested that adsorption of probe molecules can be used to determine the fraction of the surface covered with carbon.<sup>81,82</sup> Table 6 demonstrates that the fraction of the Pt surface covered with carbon on catalysts used in this study varied from 10% to 25% and was dependent on particle size. The significantly higher fractional carbon coverage after ethane hydrogenolysis on the Pt(2.9 nm)/SBA-15 catalysts is proposed to be due to the presence of a higher fraction of coordinatively unsaturated surface atoms which promote formation of irreversibly chemisorbed carbon. While this carbon was removed by oxidative treatment restoring the original surface area, it appears that under reducing conditions this carbon is irreversibly chemisorbed and most likely deposited during the first few turnovers on surface atoms with the highest coordinative unsaturation. On Pt(111), Rodriguez and Goodman have shown the amount of surface carbon after ethane hydrogenolysis in a 100 fold excess of hydrogen is temperature dependent, with the coverage increasing approximately linearly with temperature. Approximately 35% of the surface was covered with carbon as determined by Auger electron spectroscopy at 620 K.<sup>83</sup> At lower H<sub>2</sub>/C<sub>2</sub>H<sub>6</sub> ratios (H<sub>2</sub>/C<sub>2</sub>H<sub>6</sub> = 10), the coverage of the Pt(111) surface after ethane hydrogenolysis at 620 K is 60%.<sup>84</sup> The difference between the fraction of carbon coverage reported for single crystals and the Pt/SBA-15 catalysts is most likely due to the support serving as a sink for coke precursors as proposed by Parera et al.<sup>85</sup> Therefore, it is evident that reaction selectivity is structure

sensitive due to competing reaction pathways occurring at different rates on distinct surface sites.

**3.3.4. Comparison of the Reactivity of Pt/SBA-15 Catalysts Prepared by Different Synthetic Methods.** The original method, capillary inclusion (CI), developed in our laboratories for the synthesis of Pt/SBA-15 catalysts involved the incorporation of PVP-capped Pt nanoparticles into calcined SBA-15 by sonication in aqueous ethanolic solution.<sup>18</sup> PVP was removed from the Pt nanoparticle surface by calcination in oxygen by a procedure similar to that described for the NE catalysts. Adsorption uptakes on CI–Pt/SBA-15 catalysts were significantly smaller than the NE series leading to larger calculated average particle sizes. Ethylene hydrogenation rates were within a factor of 5 on both sets of catalysts with similar kinetic parameters. Ethane hydrogenolysis rates were less than a factor of 2 different on the CI series, while the NE series demonstrated a much more pronounced particle size dependence (order of magnitude for NE catalysts). The more pronounced variation is consistent with previous measurements of ethane hydrogenolysis rates on supported Pt catalysts.

This is most likely related to the larger variation in dispersion for the NE samples as determined by chemisorption. The calcination–reduction procedure was more effective removing PVP from the nanoparticle surface, or the capillary inclusion method perturbed the mesoporous oxide in a way that could not be assessed by the conventional characterization tools (TEM, SAXS, nitrogen adsorption). The smaller monolayer uptakes on the CI samples suggest that either the quantity of residual PVP is higher or the agglomeration of the particles is more severe on these samples than the NE samples. One possible explanation may be related to condensation of volatile PVP precursors during calcination on the surface of Pt particles, which may be reduced in the NE silica having pores with a slightly larger diameter. A similar explanation has recently been proposed by Chandler and co-workers<sup>35,36</sup> for differences in catalytic behavior between xerogel silica encapsulated dendrimer-templated nanoparticles and the same nanoparticles deposited on amorphous silica by impregnation. A second explanation is that the silica template polymer (Pluronic P123)

(80) Hoffman, J.; Meusel, I.; Hartmann, J.; Libuda, J.; Freund, H. J. *J. Catal.* **2001**, *204*, 378.

(81) Rivera-Latas, F. J.; Dalla Betta, R. A.; Boudart, M. *AIChE J.* **1992**, *38*, 771.

(82) Zaera, F.; Somorjai, G. A. *Langmuir* **1986**, *2*, 686.

(83) Rodriguez, J. A.; Goodman, D. W. *J. Phys. Chem.* **1990**, *94*, 5342.

(84) Zaera, F.; Somorjai, G. A. *J. Am. Chem. Soc.* **1985**, *89*, 3211.

(85) Parera, J. M.; Figoli, N. S.; Traffano, E. M.; Beltramini, J. N.; Martinelli, E. E. *Appl. Catal.* **1983**, *5*, 33.

may prevent the severe agglomeration of the particles and maintain their dispersion in the channel structure during high-temperature treatment at 723 K. Pluronic P123 is removed from CI-SBA-15 by *ex situ* calcination at 823 K for 12 h before attachment of Pt nanoparticles. Both studies demonstrate comparable reaction rates (turnover frequency) for both ethylene hydrogenation and ethane hydrogenolysis when normalized to the number of surface atoms determined by gas adsorption.

The nanoparticle encapsulation method introduced in this manuscript enables the synthesis of catalytic structures with tunable properties such as metal particle size represents an advance in catalyst synthesis. Characterization of such materials confirms that particle size can be rationally controlled during synthesis, incorporated into oxide structures, and are catalytically active after activation. Reactivity studies with these catalysts may enable the development of very accurate structure–activity and selectivity correlations in heterogeneous catalysis.

#### 4. Summary

Platinum nanoparticle supported catalysts with narrow size distributions and a highly ordered mesoporous silica matrix were prepared by *in situ* hydrothermal growth in stabilized nanoparticle aqueous solution. Resulting materials are calcined to remove stabilizing polymer from the nanoparticle surface, and amphiphilic triblock copolymers used to template the mesoporous structure. Reduction of the materials yields supported metallic nanoparticles with a high fraction of the as-synthesized particle size chemically active as determined by selective gas adsorption and infrared investigations of CO adsorption. Hydrocarbon conversion reactions confirm catalysts are active. Initial ethylene hydrogenation rates were insensitive to particle sizes in the 1–7 nm range, while ethane hydrogenolysis rates varied by 2 orders of magnitude over Pt particles within the same size range. Smaller particles were more active for hydrogenolysis suggesting that coordinatively unsaturated surface atoms prevalent in small crystallites were more reactive for C–H and C–C bond activation. CO adsorption experiments qualitatively confirm that surface site heterogeneity (*i.e.*, surface roughness) increases with decreasing particle size. The most reactive of these unsaturated sites are assumed responsible for ethane

decomposition to surface carbon during hydrogenolysis. The degree of surface carbon deposition was structure sensitive, with smaller Pt nanoparticles demonstrating higher carbon coverage after reaction. Larger particles are more selective for methane formation; smaller particles are more active for methane formation and carbon deposition. Characterization of catalysts before and after hydrogenolysis confirms that surface carbon is irreversibly chemisorbed during reaction, the amount of which depends on particle size. Surface site heterogeneity affects reaction selectivity by enabling competing reaction pathways to exist. The most significant impact of nanoscience methods on heterogeneous catalysis is in catalyst synthesis: the ability to design and control catalytic structures during synthesis which enables production of catalysts capable of specific (*i.e.*, selective) function. In the present example, the ability to synthesize monodisperse particles by solution phase reduction enables the study of intrinsic activity and selectivity of particle size rather than ensemble (particle size) averaged values of these kinetic phenomena.

**Acknowledgment.** This work was supported by the Director, Office of Energy Research, Office of Basic Energy Sciences, Chemical Sciences Division, of the U.S. Department of Energy under Contract No. DE-AC02-05CH11231. The authors acknowledge Professor M. A. Vannice of the Pennsylvania State University for the 3.2% Pt/SiO<sub>2</sub> material and Dr. Samrat Mukherjee for its preparation. R.M.R. thanks Professor Zoltan Paál for the EUROPT-1 sample. R.M.R. acknowledges the Ford Motor Company for financial support through a graduate fellowship administered by the Berkeley Catalysis Center.

**Supporting Information Available:** Details of the synthesis and characterization of the Pt/SBA-15 catalyst with Pt sols under acidic condition (Figure S1) and the synthesis and characterization of SBA-15 under acidic and neutral conditions (Figure S2 and Table S1); comparison of ethane hydrogenolysis rates as a function of particle size with those from the reported literature (Figure S3). This material is available free of charge via the Internet at <http://pubs.acs.org>.

JA057383R